Magnetic response of a highly nonlinear soliton lattice in a monoaxial chiral helimagnet

J. Kishine [1,2] and A. S. Ovchinnikov [3,4]

[1] *Division of Natural and Environmental Sciences, The Open University of Japan, Chiba 261-8586, Japan*

[2] *Institute for Molecular Science, 38 Nishigo-Naka, Myodaiji, Okazaki, 444-8585, Japan*

[3] *Institute of Natural Science and Mathematics, Ural Federal University, Ekaterinburg 620002, Russia*

[4] *Institute of Metal Physics, Ural Division, Russian Academy of Sciences, Ekaterinburg 620219, Russia*

(Received 24 January 2020; revised manuscript received 1 May 2020; accepted 4 May 2020; published 22 May 2020)

We present a theory of nonlinear magnetic response of a chiral soliton lattice state in a monoaxial chiral helimagnet under an oscillating magnetic field. The chiral soliton lattice is stabilized by a static magnetic field applied perpendicular to the chiral axis. Just below the critical field strength, where an incommensurate-to-commensurate phase transition occurs, the soliton density becomes quite low and almost isolated 2π kinks are partitioned by vast ferromagnetic regions. We consider this highly nonlinear regime and demonstrate that internal deformations of each kink give rise to the nonlinear response in this regime.

DOI: 10.1103/PhysRevB.101.184425

I. INTRODUCTION

Nonlinear magnetic response to an oscillating field provide useful information for understanding physical properties of magnetic compounds. This powerful magnetic diagnostics is conventionally used to elucidate dynamic responses of magnetic domains in ferromagnets [1] in addition to allowing the determination of the phase transition temperature [2]. This experimental technique has applications in studies of low-field magnetic hysteresis of ferromagnetic [3,4] and helimagnetic materials [5,6], nonlinear responses in ferroelectrics [7], and molecule-based magnets with structural chirality [8,9]. Another broad research area involves studies of nonlinear susceptibility in the vicinity of spin glass transition temperature [10–12]. A chirality-driven mechanism due to fluctuations of a dynamical noncollinear spin order variable, which, defined as a vector product of two nearest-neighbor lattice spins, was proposed to explain new universality classes of experimentally observed spin-glass critical phenomena [13–17].

Recent investigations of chiral magnets have become a new landmark of the nonlinear response applications. These materials comprise both the chirality of critical fluctuations, such as in the case of MnSi [18,19], and the ac magnetic responses of magnetic domains found, for example, in $CrNb_3S_6$ [20]. In the latter case, the phase diagram of the chiral helimagnet as a function of temperature T and a steady magnetic field H_{dc} was constructed by means of the oscillating magnetic susceptibility measurements. It was revealed that when $H_{dc} = 0$ the ac response consists of a giant third-order harmonic component ($M_{3\omega}$) along with a first-order part ($M_{1\omega}$) at the transition between the chiral helimagnetic (CHM) state to the paramagnetic (PM) state. The nonzero dc field applied perpendicular to the helical axis transforms the CHM state in favor of the chiral soliton lattice (CSL) state. At small H_{dc}, ferromagnetic regions are poorly expressed against the predominant magnetic helicoidal order. For this regime, it was found that the $M_{3\omega}$ is drastically suppressed, i.e., the transition between the CSL and the PM states is characterized only by a linear magnetic response. At higher dc fields, the ferromagnetic areas start to grow that allows the CSL state to be viewed as a regular arrangement of 2π kinks in the ferromagnetic background. The order is known as the highly nonlinear CSL. With increasing temperature, it transforms into the forced ferromagnetic (FFM) state, and eventually the PM state is reached. The transition between the CSL state and the FFM states is again accompanied by a large $M_{3\omega}$ as well as a complex $M_{1\omega}$, whereas the FFM-PM transition gives rise a linear magnetic response without any energy loss. These data reported by Mito *et al.* [20] were supplemented by a comprehensive study made by Clements *et al.* [21]. They could trace the steady magnetic field dependence of the oscillating magnetic response for the first five harmonic components and have amply demonstrated a presence of the noticeable $M_{2\omega}$ component as the ferromagnetic-domain-rich CSL evolves into the FFM state. In small ac fields, the $M_{2\omega}$ is connected to the breaking of the time inversion symmetry, and the large signal reflects the presence of spontaneous magnetization [2]. The $M_{3\omega}$, in contrast, is associated with the microscopic breaking of spatial symmetry of magnetic moments [8], thereby confirming the presence of the ferromagnetic regions in the highly nonlinear CSL state.

The peculiarities discovered in the nonlinear response are closely linked to the H-T phase diagram of the chiral helimagnet $CrNb_3S_6$, detailed structure thereof is still actively debated. The nature of the possible phase transitions has been addressed both experimentally and theoretically. The dc magnetization and magnetic entropy change measurements [22,23] testify apparently a second-order phase transition to the FFM state at magnetic fields above the critical field of the incommensurate-commensurate (IC-C) phase transition. At moderate and low magnetic fields the onset of the chiral IC phase was detected, including crossover between the nonlinear and highly nonlinear regions of the CSL state along with complementary crossover between the CHM and CSL states.

These investigations also confirm the existence of the weakly nonlinear CSL and the concurrent disappearance of the CHM phase for small nonzero applied fields in temperature region above and below the Curie temperature $T_c \approx 130.7$ K. A possibility of first-order behavior at the phase transition in small magnetic fields were also argued. The metamagnetic crossover from the weakly nonlinear to the highly nonlinear CSL regime has been verified by measurements of magnetoresistance [24]. The theoretical studies by Laliena *et al.* [25,26] predict a transition line between the highly nonlinear CSL and the FFM states at low temperature and high dc fields as being of second-order (continuous) nucleation type transition [27]. The boundary between the CHM and the PM state may be categorized as the second-order instability-type transition [28] according to de Gennes classification. The second-order line sections are separated by a line of first-order transitions with two tricritical end points as a terminus at intermediate temperatures and magnetic fields. Experimental validation of these tricritical points remains controversial [29]. Another example of the nucleation-type transition are the transition at the lower critical field of type-II superconductors and the cholesteric-to-nematic transition in liquid crystals. The former analogy was discussed in Refs. [30,31], where a similarity between the monoaxial chiral helimagnet and type-II superconductors was pointed out for a surface barrier.

In our work we present the theory of nonlinear magnetic response to an oscillating field for the highly nonlinear regime of the chiral soliton lattice. The state emerging as a result of crossover under increasing the steady magnetic field perpendicularly to the chiral axis may be regarded as a regular arrangement of nearly isolated 2π kinks partitioned by vast ferromagnetic regions. It is separated from the FFM state by the nucleation-type continuous transition and may be modeled as particles that repel each other by a force, which decay exponentially as a distance between the kinks increases [32]. Then, it is appropriate to assume that each of the kinks reacts independently from the other ones to the external oscillating field. These considerations are supported by observation that the Lamé potential resulting from the CSL consists of a periodic array of modified Pöschl-Teller potentials [33,34]. We argue that the appearance of high-order harmonics and phase shifts is related to quasilocalized excitations triggered by internal deformations of the separate kink.

To provide support for the picture presented above we formulate a model of the magnetic soliton lattice relevant for the chiral helimagnet $CrNb_3S_6$ and explain how crossover between the weakly and highly nonlinear CSL regimes originates from Fourier decomposition of the CSL configuration. Furthermore, we find spectrum of Gaussian fluctuations of a single kink, thereby specifying its internal deformations. Using the spectrum, a Lagrangian formalism based on the collective coordinate method [34–36] is developed to describe kink dynamics driven by an external oscillating magnetic field. Solving of the corresponding dynamical equations is reduced to a challenge how to get periodic (Floquet) solutions. We apply the algorithm elaborated by Erugin [37] to successfully overcome the problem and use the periodic solutions to recover higher-order harmonic components of magnetization together with related phase shifts. Our analysis reveals that the order parameter that characterizes the second-order phase transition of the nucleation type, namely a density of kinks, has a crucial role to play in hierarchy of these higher-order harmonic components. This allows us to establish the limits of our theory and predicts the onset of the linear response regime while approaching the FFM phase boundary.

This paper is organized as follows. In Sec. II, we describe the model and summarize key details of the ground state and the excitations of the highly nonlinear CSL state. Here, the Lagrangian formalism to describe dynamics of a single kink is presented. In Sec. III, the periodic solution of the dynamical equations is looked for which is used to derive higher-order harmonics of nonlinear magnetic response. The conclusions are given in Sec. IV.

II. MODEL

The layered structure of $CrNb_3S_6$ consists of 2H-type planar NbS_2 with the Cr atoms intercalated between the planes and belongs to the noncentrosymmetric hexagonal space group $P6_322$ [38]. The localized moments of the Cr^{3+} ions (the spin $S = 3/2$) are oriented in the crystallographic *ab* plane and exhibit strong single-ion anisotropy [39,40]. As has been repeatedly proven the one-dimensional (1D) model of the chiral soliton lattice [41] explains properties of the compound beautifully that was amply confirmed by Togawa *et al.* via the Lorentz microscopy experiments [42].

In the continuum approximation, the monoaxial chiral helimagnet is described by the Hamiltonian density

$$\mathcal{H} = \frac{JS^2 a_0}{2}[(\partial_z\theta)^2 + \sin^2\theta(\partial_z\varphi)^2] - DS^2\sin^2\theta(\partial_z\varphi) - HSa_0^{-1}\sin\theta\cos\varphi, \tag{1}$$

where a_0 is the lattice constant and the semiclassical spin

$$\boldsymbol{S}(z) = S[\sin\theta(z)\cos\varphi(z), \sin\theta(z)\sin\varphi(z), \cos\theta(z)]$$

is specified by the spherical coordinates. Here, $J > 0$ is the strength of the nearest-neighbor ferromagnetic exchange coupling. The monoaxial DM vector $\boldsymbol{D} = D\hat{\boldsymbol{e}}_z$ directed along the z axis is parametrized by the constant D. To stabilize the CSL state, a static magnetic field H, measured in units $g\mu_B$, is applied perpendicularly to the z axis.

The CSL ground state is given by $\theta_0 = \pi/2$ and $\varphi_0(z) = \pi + 2\mathrm{am}(\bar{z})$, where the dimensionless coordinate $\bar{z} = (m/\kappa)z$ is introduced with $m^2 = H/(a_0^2 JS)$. The $\mathrm{am}(\ldots)$ is the Jacobi amplitude function depending on the elliptic modulus κ ($0 \leqslant \kappa \leqslant 1$). The modulus κ is determined by minimizing an energy that gives $\kappa = 4mE/\pi q_0$, where $q_0 = D/a_0 J$, and the CSL spatial period, $\lambda_{\mathrm{CSL}} = 2\kappa K/m$, with K and E being the elliptic integrals of the first and second kind, respectively.

The CSL undergoes a continuous transition to the forced ferromagnetic state above the critical field

$$H_c = \left(\frac{\pi q_0 a_0}{4}\right)^2 JS \tag{2}$$

attained as $\kappa \to 1$. The evolution of the CSL upon increasing H is schematically shown in Fig. 1.

A convenient way to trace this evolution from weakly to highly nonlinear regimes is provided by unpolarized neutron

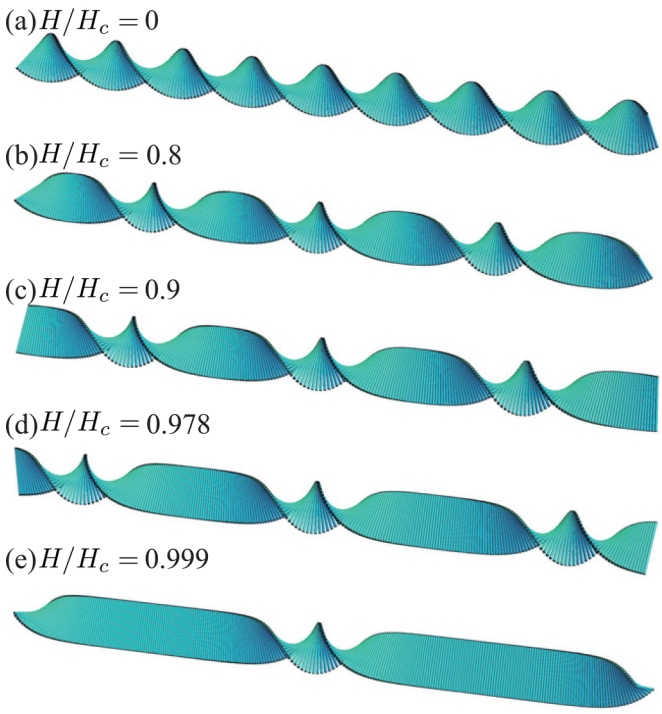

FIG. 1. Formation of the chiral soliton lattice for (a) $H/H_c = 0.8$, (b) 0.9, (c) 0.978, and (d) 0.999.

scattering [43]. The cross section of scattered neutrons

$$\frac{d\sigma}{d\Omega} \propto \sum_n \delta(\mathbf{q} - n\mathbf{G}_{\rm CSL})|\mathbf{S}_\mathbf{q}^\perp|^2$$

depends on the Fourier transform of the magnetization component $\mathbf{S}_\mathbf{q}^\perp$ perpendicular to the chiral axis on condition that the scattering vector $\mathbf{q} = (0, 0, q)$ is parallel to this axis. Here, $\mathbf{G}_{\rm CSL} = (0, 0, G_{\rm CSL})$, $G_{\rm CSL} = 2\pi/\lambda_{\rm CSL}$, is the wave vector related to the CSL.

By using the Fourier series of the CSL configuration

$$\cos\varphi_0(z) = 1 + 2\left(\frac{E-K}{\kappa^2 K}\right) + \frac{2\pi^2}{\kappa^2 K^2}\sum_{n=1}^{\infty}\frac{n\cos(n\pi\bar{z}/K)}{\sinh(n\pi K'/K)}, \tag{3}$$

$$\sin\varphi_0(z) = \frac{2\pi^2}{\kappa^2 K^2}\sum_{n=1}^{\infty}\frac{n\sin(n\pi\bar{z}/K)}{\cosh(n\pi K'/K)} \tag{4}$$

with $\pi\bar{z}/K = 2\pi/\lambda_{\rm CSL}$, the cross section may be presented as

$$\frac{d\sigma}{d\Omega} \propto \sum_{n=-\infty}^{+\infty} C_n\delta(q - nG_{\rm CSL}),$$

where

$$C_0 = \left\{1 + 2\left(\frac{E-K}{\kappa^2 K}\right)\right\}^2 \tag{5}$$

is the weight of the ferromagnetic component, and

$$C_n = \left(\frac{\pi}{\kappa K}\right)^4\left\{\frac{n^2}{\sinh^2\left(n\frac{\pi K'}{K}\right)} + \frac{n^2}{\cosh^2\left(n\frac{\pi K'}{K}\right)}\right\} \tag{6}$$

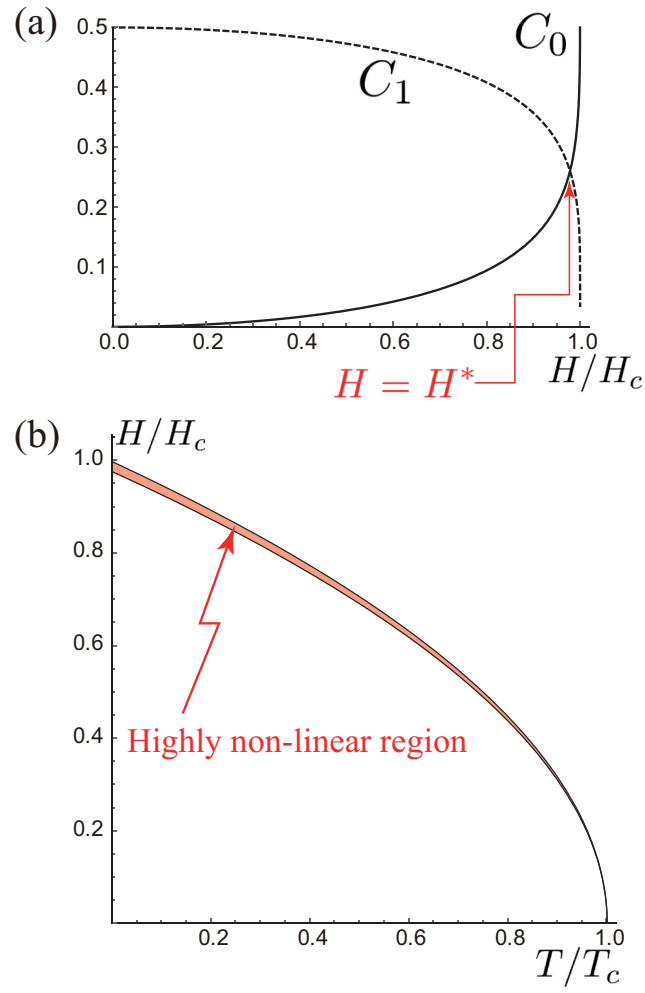

FIG. 2. (a) Dependence of C_0 and C_1 on H/H_c. They intersect at $H = H^*$. (b) Schematic phase diagram where H_c and H^* are indicated as functions of T. The narrow region $H^* < H < H_c$ is identified with highly nonlinear region.

is that of spatially modulated components. Here, K' denotes the complete elliptic integral of the first kind with the complementary elliptic modulus $\kappa' \equiv \sqrt{1-\kappa^2}$.

The ratio C_0/C_1 serves as an indicator of nonlinearity in the CSL structure. The weight C_1 corresponds to the spiral modulation, while C_0 indicates a presence of the ferromagnetic areas. The dominance of C_0 over C_1 means the onset of the nonlinear regime [44]. In Fig. 2(a), we show the field dependence of the C_0 and C_1. It is seen that C_0/C_1 exceeds the unity at $H^*/H_c \simeq 0.978$. This value determines crossover between the linear and the highly nonlinear CSL states [26], i.e., the latter becomes conspicuous only in the vicinity of the critical field H_c [see Fig. 1(e)].

To gain insight into the appearance of the crossover line on the field-temperature phase diagram, we replace S with a simple mean-field form having the temperature dependence, $\sqrt{1-T/T_c}$, where T_c denotes the transition temperature at zero field. Inserting this form into Eq. (2), we acquire the temperature-dependent critical field $H_c(T) = H_c(0)\sqrt{1-T/T_c}$. On the other hand, it can be assumed that the crossover value $H^*(T)/H_c(T)$ is independent of

temperature that brings forth the conceptual phase diagram shown in Fig. 2(b). We note that the highly nonlinear regime occupies a quite narrow region bounded by $H^*(T) < H < H_c(T)$.

A. Spectrum of fluctuations

Below, we thoroughly discuss fluctuations around the soliton lattice ground state,

$$\varphi(z) = \varphi_0(z) + \delta\varphi(z), \tag{7}$$

$$\theta(z) = \frac{\pi}{2} + \delta\theta(z). \tag{8}$$

By expanding the Hamiltonian (1) up to the second order with respect to the $\delta\varphi$ and $\delta\theta$, we obtain $\mathcal{H}[\varphi,\theta] = \mathcal{H}[\varphi_0] + \delta\mathcal{H}$, where

$$\delta\mathcal{H} = \frac{JS^2a_0}{2}\int dz(\delta\varphi\hat{\Lambda}_\varphi\delta\varphi + \delta\theta\hat{\Lambda}_\theta\delta\theta). \tag{9}$$

Here, the linear differential operators are given by

$$\hat{\Lambda}_\varphi = -\left(\frac{m}{\kappa}\right)^2\left(\partial_{\bar{z}}^2 - 2\kappa^2\mathrm{sn}^2\bar{z} + \kappa^2\right), \tag{10}$$

and

$$\hat{\Lambda}_\theta = \hat{\Lambda}_\varphi + \Delta(z) \tag{11}$$

with

$$\Delta(z) = -4q_{\mathrm{CSL}}^2\mathrm{dn}^2\bar{z} + 4q_0q_{\mathrm{CSL}}\mathrm{dn}\bar{z} \tag{12}$$

being the energy gap function of the θ mode originated from the DM interaction. Here, $q_{\mathrm{CSL}} = 2K/\lambda_{\mathrm{CSL}}$ is the wave number of the CSL structure.

The physical situation of a single kink inside of a ferromagnetic matrix corresponds to the highly nonlinear regime achieved when $\kappa \to 1$. In this case, the CSL solution degenerates into

$$\varphi_0(\bar{z}) \longrightarrow 2\pi - 2\cos^{-1}(\tanh\bar{z}), \tag{13}$$

where $\bar{z} = 2z/l_0$ with $l_0 = 8/\pi q_0$ being the width of the kink localization (see the inset of Fig. 4).

We stress our analysis applies to the magnetic fields just below the critical field of the IC-C phase transition, $H < H_c$, when kinks become energetically preferred globally compared to the field polarized state. This means that any such kink is placed deeply inside within the bulk opposite to the scenario of edge instabilities considered in Refs. [30,45], when the center of the kink is positioned outside of the sample. The latter approach is valid for fields larger than the critical one, $H > H_c$, when the kink, being a local excitation of the field polarized state, triggers creation of a helical phase, which penetrates the forced ferromagnetic phase within the bulk. Then, the operators (10) and (11) take the form

$$\hat{\Lambda}_\varphi \to \left(\frac{\pi q_0}{4}\right)^2\left(-\partial_{\bar{z}}^2 - 2\mathrm{sech}^2\bar{z} + 1\right), \tag{14}$$

$$\hat{\Lambda}_\theta \to \left(\frac{\pi q_0}{4}\right)^2\left(-\partial_{\bar{z}}^2 - 6\mathrm{sech}^2\bar{z} + \frac{16}{\pi}\mathrm{sech}\bar{z} + 1\right). \tag{15}$$

Figure 3 illustrates the potentials for the φ fluctuations, $V_\varphi(\bar{z}) = -2\mathrm{sech}^2\bar{z} + 1$, and the θ fluctuations, $V_\theta(\bar{z}) = -6\mathrm{sech}^2\bar{z} + (16/\pi)\mathrm{sech}\,\bar{z} + 1$, where we present additionally the gap function, $\Delta(\bar{z}) = V_\theta(\bar{z}) - V_\varphi(\bar{z})$, at $\kappa = 1$. Notice that the potentials V_φ and V_θ, being expanded around their minima, result in parabolic potentials what could be a reason of linear response but fails to explain nonlinear effects. Therefore, a more detailed treatment of the problem should be undertaken.

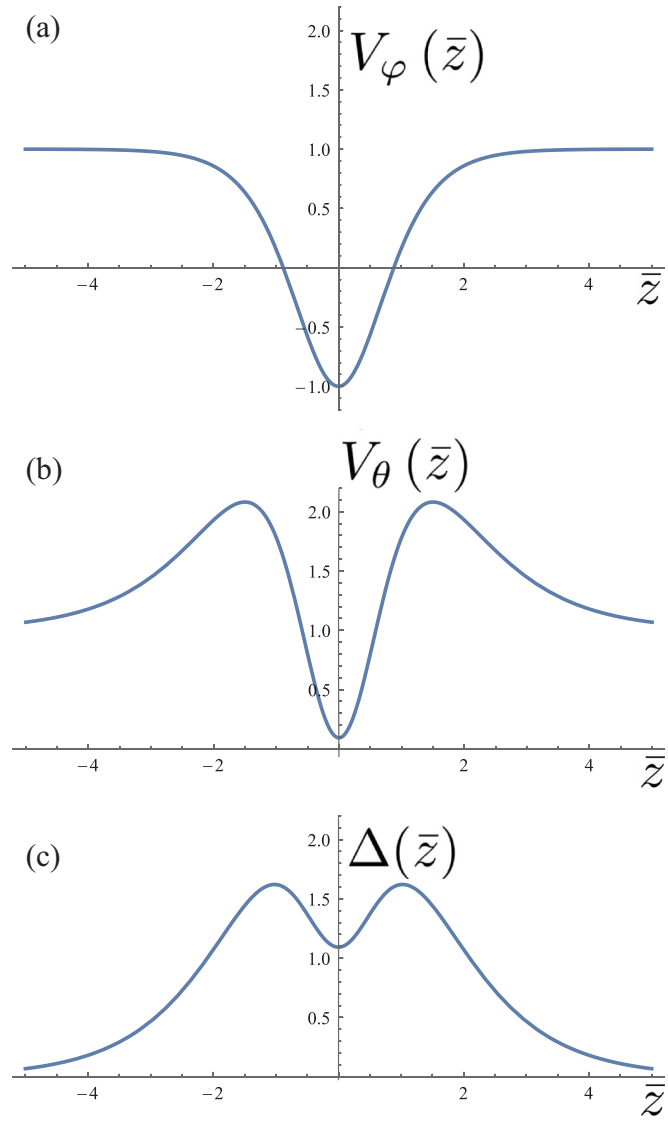

FIG. 3. Spatial profiles of the potentials for (a) the φ fluctuation, (b) θ fluctuation, and (c) the gap for the θ fluctuation, for the limiting case $\kappa \to 1$.

The Schrödinger-type operator $\hat{\Lambda}_\varphi$ involves the Pöschl-Teller potential defined by $U_0(\bar{z}) = -l(l+1)\mathrm{sech}^2(\bar{z})$ with the particular value $l = 1$. For further analysis, the most important being a presence of the single bound state $\Phi_0 = 2^{-1/2}\mathrm{sech}(\bar{z})$ with the eigenvalue $\varepsilon_0^{(\varphi)} = 0$ (zero mode) [46].

Unfortunately, the operator $\hat{\Lambda}_\theta$ does not permit a similar treatment. However, it may be shown through the WKB formalism (see Appendix A) that there is a quasilocalized state u_0 with the energy $\varepsilon_0^{(\theta)}$, $\hat{\Lambda}_\theta u_0(\bar{z}) = \varepsilon_0^{(\theta)}u_0(\bar{z})$. By using Eqs. (A11), (A12) we get $\varepsilon_0^{(\theta)} \approx 0.0254$ provided $q_0 = 0.16a_0^{-1}$. Numerov's algorithm yields $\varepsilon_0^{(\theta)} \approx 0.0256$. We

neglect henceforth the tunneling process giving a finite width of the state.

B. Lagrangian

Our target is to obtain equations of motion of the isolated kink in the ferromagnetic surrounding based on the fluctuation spectra discussed above. The Lagrangian density includes three terms,

$$\mathcal{L} = \mathcal{L}_{\rm kin} + \mathcal{L}_{\rm fluct} + \mathcal{L}_{\rm Zeeman} \tag{16}$$

such as the kinematic part [47] associated with the Berry phase

$$\mathcal{L}_{\rm kin} = \frac{\hbar S}{a_0}\int_{-L/2}^{L/2} dz[\cos\theta(z) - 1]\partial_t\varphi(z), \tag{17}$$

the part related to the energy of fluctuations,

$$\mathcal{L}_{\rm fluct} = \frac{JS^2}{2a_0}\int_{-L/2}^{L/2} dz\{\delta\varphi(z)\hat{\Lambda}_\varphi\delta\varphi(z) + \delta\theta(z)\hat{\Lambda}_\theta\delta\theta(z)\}, \tag{18}$$

and the Zeeman coupling with the oscillating field, $H_x(t) = h_0\sin(\Omega t)$, of the strength h_0 and the frequency Ω,

$$\mathcal{L}_{\rm Zeeman} = -\frac{S}{a_0}H_x(t)\int_{-L/2}^{L/2} dz\sin\theta(z)\cos\varphi(z). \tag{19}$$

Integration runs over the interval $[-L/2, L/2]$ that has the kink at the center.

In the method of collective coordinates the dynamics is fully described by two variables, the center-of-mass position $Z(t)$ and the out-of-plane quasizero mode coordinate $\xi_0(t)$

$$\varphi(z,t) = \varphi_0[z - Z(t)], \tag{20}$$

$$\theta(z,t) = \pi/2 + \xi_0(t)u_0[z - Z(t)], \tag{21}$$

where u_0 is not periodic on $[-L/2, L/2]$ (see Fig. 6).

To obtain equations of motion in the context of the collective coordinates we expand the Lagrangian (16) in terms of ξ and Z, which are assumed to be small as long as the oscillating field is weak. In this way, we get

$$\mathcal{L} \simeq K_1\xi_0(t)\dot{Z}(t) - \frac{JS^2}{2a_0}\varepsilon_0^{(\theta)}\xi_0^2(t) + K_2H_x(t)Z^2(t) + K_3H_x(t)\xi_0^2(t), \tag{22}$$

where

$$K_1 = \frac{\hbar S}{a_0}\int_{-L/2}^{L/2} dz u_0(z)\partial_z\varphi_0(z), \tag{23}$$

$$K_2 = \frac{S}{2a_0}\int_{-L/2}^{L/2} dz\{\cos\varphi_0(z)[\varphi_0'(z)]^2 + \sin\varphi_0(z)\varphi_0''(z)\}, \tag{24}$$

$$K_3 = \frac{S}{2a_0}\int_{-L/2}^{L/2} dz u_0^2(z)\cos\varphi_0(z) \tag{25}$$

and it is taken into consideration that the sliding coordinate Z corresponds to the zero mode of φ excitations with $\varepsilon_0^{(\varphi)} = 0$. On the other hand, the θ excitations acquire a finite energy gap $\varepsilon_0^{(\theta)} = S^2D^2/2a_0J$.

The equations of motion for the collective coordinates are then given by

$$\frac{d\xi_0(t)}{dt} = \frac{2K_2}{K_1}h_0\sin(\Omega t)Z(t),$$
$$\frac{dZ(t)}{dt} = \frac{JS^2\varepsilon_0^{(\theta)}}{K_1a_0}\xi_0(t) - \frac{2K_3}{K_1}h_0\sin(\Omega t)\xi_0(t). \tag{26}$$

To account of the Gilbert damping specified by the constant γ the Rayleigh dissipation function may be used [35,46]

$$\mathcal{W} = \frac{\gamma\hbar S}{2a_0}(\mathcal{M}\dot{Z}^2 + \dot{\xi}_0^2),$$

where $\mathcal{M} = \int_{-L/2}^{L/2} dz[\partial_z\varphi_0(z)]^2$.

It modifies Eqs. (26) as

$$\frac{d\xi_0(t)}{dt} = \frac{2K_2}{K_1}h_0\sin(\Omega t)Z(t) - \frac{\gamma\hbar S\mathcal{M}}{K_1a_0}\dot{Z}(t),$$
$$\frac{dZ(t)}{dt} = \frac{JS^2\varepsilon_0^{(\theta)}}{K_1a_0}\xi_0(t) - \frac{2K_3}{K_1}h_0\sin(\Omega t)\xi_0(t) + \frac{\gamma\hbar S}{K_1a_0}\dot{\xi}_0(t). \tag{27}$$

Thus, the Gilbert damping leads to the linear terms in the equations of motion and does not relate directly to mechanism of nonlinear response. We neglect this effect in further consideration.

III. FLOQUET SOLUTION AND NONLINEARITY

A. Floquet solution

To find a Floquet solution of these equations of motion it is convenient to define the integral matrix composed from two linearly independent solutions

$$X = \begin{pmatrix} \xi_0^{(1)} & Z^{(1)} \\ \xi_0^{(2)} & Z^{(2)} \end{pmatrix}. \tag{28}$$

Then, the system (26) may be recast into the form

$$\frac{dX}{d\tau} = XP(\tau), \tag{29}$$

where $P(\tau) = P_0 + h_0P_1(\tau)$,

$$P_0 = \begin{pmatrix} 0 & \rho \\ 0 & 0 \end{pmatrix}, \quad P_1 = \begin{pmatrix} 0 & -\beta \\ \alpha & 0 \end{pmatrix}\sin\tau$$

with

$$\rho = JS^2\varepsilon_0^{(\theta)}/(a_0\Omega K_1), \tag{30}$$

$$\alpha = 2K_2/(\Omega K_1), \tag{31}$$

$$\beta = 2K_3/(\Omega K_1). \tag{32}$$

Here, the time $\tau = \Omega t$ is introduced. It is to be noted that ρ, α, and β are inversely proportional to Ω [48].

A way of constructing Floquet solution of Eq. (29) is explained in the Appendix B. This method is based on the fact that in the representation of the integral matrix

$$X(\tau) = \exp(W\tau)N(\tau) \tag{33}$$

the W and N may be expanded as the series with respect to the small parameter h_0, that appears in the coefficients of the system (29). In our analysis the series are limited to third order

$$W \approx W_0 + h_0 W_1 + h_0^2 W_2 + h_0^3 W_3, \tag{34}$$

$$N(\tau) \approx N_0(\tau) + h_0 N_1(\tau) + h_0^2 N_2(\tau) + h_0^3 N_3(\tau). \tag{35}$$

Following the procedure set out in Appendix C one may find consistently $W_0 = P_0$ and $N_0 = I$ [see, Eqs. (B5), (B6)]. The explicit forms of W_1 and $N_1(\tau)$ are originated from Eqs. (B8), (B7), and Eq. (B9), respectively,

$$W_1 = \begin{pmatrix} -\alpha\rho & 0 \\ 0 & \alpha\rho \end{pmatrix}, \tag{36}$$

$$N_1(\tau) = \begin{pmatrix} \alpha\rho\sin\tau & (\beta - 2\alpha\rho^2)(\cos\tau - 1) \\ \alpha(1-\cos\tau) & -\alpha\rho\sin\tau \end{pmatrix}. \tag{37}$$

Reiterating steps of the algorithm for terms of second and third orders (see Appendix C for details) we obtain the matrix W

$$W = \begin{pmatrix} -\frac{5}{12}(7\alpha^3\rho^3 - 4\alpha^2\beta\rho)h_0^3 - \alpha\rho h_0 & \frac{1}{4}(5\alpha^2\rho^3 - 6\alpha\beta\rho)h_0^2 + \rho \\ -\frac{3}{2}\alpha^2 h_0^2\rho & \frac{5}{12}(7\alpha^3\rho^3 - 4\alpha^2\beta\rho)h_0^3 + \alpha\rho h_0 \end{pmatrix}. \tag{38}$$

It has purely imaginary characteristic numbers that yields

$$\exp(W\tau) = \cos(\lambda\tau)I + \frac{1}{\lambda}\sin(\lambda\tau)W, \tag{39}$$

with

$$\lambda = \frac{1}{\sqrt{2}}\left[\alpha\rho h_0 - \frac{1}{24}h_0^3(95\alpha^3\rho^3 - 26\alpha^2\beta\rho)\right],$$

and the integral matrix X turns out to be oscillatory as a result.

By carrying out direct calculation of Eq. (33) and ignoring a frequency shift to the value $\lambda \ll 1$, we get eventually the periodic Floquet solution (D3), (D4), see Appendix D for details.

B. Magnetization

The resultant magnetization is originated from dependence on the collective coordinates

$$\begin{aligned} M_x(t)/M_0 &= \int_{-L/2}^{L/2}\frac{dz}{a_0}\sin\theta(z,t)\cos\varphi(z,t) \\ &= \int_{-L/2}^{L/2}\frac{dz}{a_0}\cos\{\xi_0(t)u_0[z - Z(t)]\}\cos\{\varphi_0[z - Z(t)]\}, \end{aligned} \tag{40}$$

where M_0 is the magnetization amplitude.

Performing expansion in powers of $\xi^m Z^n$ right up to third order ($m + n \leqslant 3$), we obtain the fluctuation part,

$$\delta M_x/M_0 = -\frac{a}{2}Z^2 - \frac{b}{2}\xi_0^2 + \frac{c}{6}Z^3 + \frac{f}{2}Z\xi_0^2, \tag{41}$$

where

$$a = \int_{-L/2}^{L/2}\frac{dz}{a_0}\left\{\varphi_0''(z)\sin\varphi_0(z) + \varphi_0'^2\cos\varphi_0(z)\right\}, \tag{42}$$

$$b = \int_{-L/2}^{L/2}\frac{dz}{a_0}u_0(z)^2\cos\varphi_0(z), \tag{43}$$

$$c = \int_{-L/2}^{L/2}\frac{dz}{a_0}\left\{\begin{matrix}\varphi_0^{(3)}(z)\sin\varphi_0(z) - \varphi_0'^3\sin\varphi_0(z) \\ +3\varphi_0'(z)\varphi_0''(z)\cos\varphi_0(z)\end{matrix}\right\}, \tag{44}$$

$$f = \int_{-L/2}^{L/2}\frac{dz}{a_0}\left\{\begin{matrix}2u_0(z)u_0'(z)\cos\varphi_0(z) \\ -u_0(z)^2\varphi_0'(z)\sin\varphi_0(z)\end{matrix}\right\}. \tag{45}$$

It follows on parity grounds that $c = 0$ and $f = 0$, note also that $a = 2K_2/S$ and $b = 2K_3/S$.

By plugging the solutions (D3), (D4) obtained earlier in (41) and neglecting higher-order terms the magnetization as function on time may be presented as follows:

$$\delta M_x(t)/M_0 = \sum_{n=1}^{3} M_{n0}\sin(n\Omega t + \delta_n). \tag{46}$$

Here, the nth-harmonic components, $n = 1, \ldots, 3$, are given by

$$M_{10} = |a\alpha\rho|h_0, \tag{47}$$

$$M_{20} = \tfrac{1}{8}|\alpha(2a\beta - 2b\alpha + 3a\alpha\rho^2)|h_0^2, \tag{48}$$

$$M_{30} = \tfrac{1}{72}\alpha^2|\rho(13a\beta - 9b\alpha + 5a\alpha\rho^2)|h_0^3. \tag{49}$$

We note that M_{10}, M_{20} are proportional to Ω^{-2}, while M_{30} to Ω^{-4}, since ρ, α, and β are inversely proportional to Ω.

The expressions for

$$\delta_1 = \tan^{-1}\left[\frac{h_0(-a\beta + b\alpha + 2a\alpha\rho^2)}{a\rho}\right], \tag{50}$$

$$\delta_2 = \tan^{-1}\left[\frac{(2a\beta - 2b\alpha + 3a\alpha\rho^2)}{\alpha\rho h_0(2a\beta + 2b\alpha - 11a\alpha\rho^2)}\right], \tag{51}$$

and $\delta_3 = 0$ determine the phase delay of each M_{n0} against the ac field.

Given the characteristic length of the kink localization, l_0, and taking the size of the system as $L/2 = Nl_0 = 8N/\pi q_0 = 8JNa_0/\pi D \propto Na_0$ we obtain

$$K_1 \sim \frac{\hbar S}{a_0}\frac{1}{\sqrt{L}}\int_{-L/2}^{L/2}\partial_z\varphi_0(z)dz = \frac{\hbar S}{a_0}\frac{2\pi}{\sqrt{L}} \sim \hbar S a_0^{-3/2}N^{-1/2}, \tag{52}$$

$$\begin{aligned} K_2 &= \frac{S}{2a_0}\int_{-L/2}^{L/2}dz\frac{d}{dz}\{\varphi_0'(z)\sin\varphi_0(z)\} \\ &= \frac{S}{a_0}\left(\frac{\pi q_0}{2}\right)\mathrm{sech}2N \sim S a_0^{-2}\mathrm{sech}2N, \end{aligned} \tag{53}$$

$$K_3 \sim \frac{S}{2a_0}\int_{-L/2}^{L/2}dz u_0^2(z)\cos\varphi_0(z) \sim S a_0^{-1}, \tag{54}$$

where we used $u_0 \sim 1/\sqrt{L}$ (see Ref. [46]) and $\sin\varphi_0(L/2) \sim 1$. We note the parameters a and b have the same dependence on N with K_2 and K_3, respectively.

By using the values for $CrNb_3S_6$ as $S = 3/2$, $J = 18$ K (or 2.484×10^{-22} J), $a_0 = 1.212 \times 10^{-9}$ m. As for the oscillating

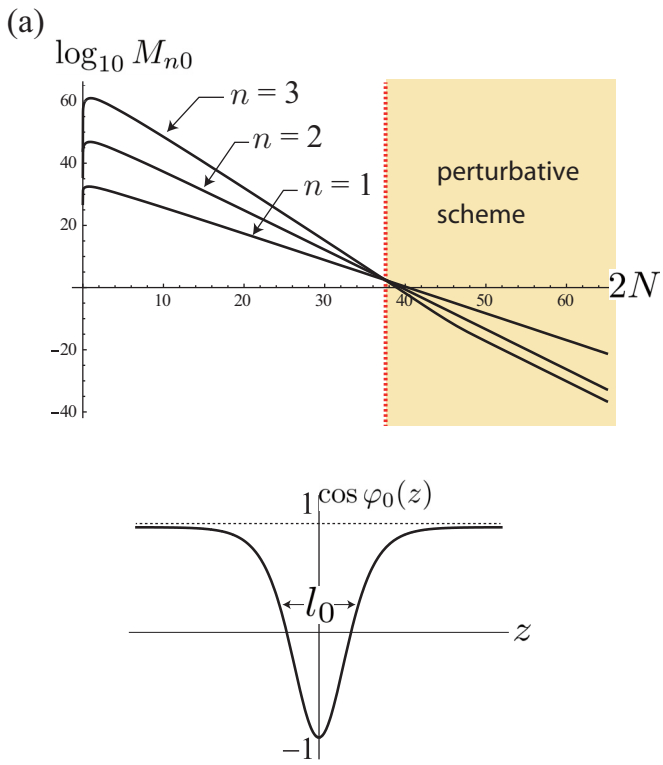

FIG. 4. Scale behavior of the amplitude M_{n0} $(n = 1, 2, 3)$ with a growth of $L/a_0 \sim 2N$. The dotted vertical line marks an onset of applicability of the perturbation analysis. The inset shows the spatial profile of a single kink with $l_0 = 8/\pi q_0$ being the width of the kink localization.

magnetic field, we follow Ref. [20] and take $h_0 = 5$ Oe (then $g\mu_B h_0 = 9.274 \times 10^{-27}$ J) and $\nu = 2\pi\Omega = 10$ Hz (then $h\nu = 6.626 \times 10^{-33}$ J). These vales lead to order-of-magnitude estimate,

$$\alpha h_0 = 2K_2 h_0/(\Omega K_1) \sim 10^{10}\sqrt{N}\,\mathrm{sech}(2N), \tag{55}$$

$$\beta h_0 = 2K_3 h_0/(\Omega K_1) \sim 10\sqrt{N}, \tag{56}$$

$$\rho = JS^2\varepsilon_0^{(\theta)}/(a_0\Omega K_1) \sim 10^4\sqrt{N}. \tag{57}$$

Plugging them into Eqs. (47)–(49), we see that the harmonic components obey the scaling laws with respect to N as

$$M_{10} \sim 10^{33} N\,\mathrm{sech}^2(2N), \tag{58}$$

$$M_{20} \sim 10^{48} N^2\,\mathrm{sech}^3(2N), \tag{59}$$

$$M_{30} \sim 10^{62} N^3\,\mathrm{sech}^4(2N). \tag{60}$$

We show the N dependence of $\log_{10} M_{n0}$ in Fig. 4. By choosing the characteristic length per the kink, $L/a_0 \sim 2N$, as $2N = 41$, we obtain the proportion close to that observed in the experiment $M_{10} \sim 0.2728$, $M_{20} \sim 0.0131$ and $M_{30} \sim 0.0003$. The corresponding phase shifts are $\delta_1 \sim 0.251$ and $\delta_2 \sim -1.132$.

It is seen that as functions of N, the amplitudes of higher harmonic contributions, M_{20} and M_{30} dominate M_{10} for smaller $2N \lesssim 40$, which indicates that the perturbative scheme [expansions given in Eqs. (34) and (35)] breaks down. Because larger $2N$ means lower kink density, our scheme works for the regime of smaller kink density specified by $2N \gtrsim 40$. This condition is consistent with the situation where the highly nonlinear regime is near the boundary of the nucleation transition [see Fig. 2(b)].

IV. CONCLUSION AND DISCUSSIONS

Measurements of dynamical magnetic response in $CrNb_3S_6$ provide exciting challenges that need to be addressed theoretically. One area of research is focused on spin resonance measurements [49,50] that find an explanation within the theory of standing spin waves in a finite-size chiral soliton lattice [51]. Other area of these studies involves oscillating magnetic susceptibility measurements, which reveal a strong presence of higher-order harmonic components of magnetization near the incommensurate-commensurate phase transition and which still remain unexplained. Low frequencies of the ac field used in these experiments, 10–10^4 Hz, lie far below the spin resonance frequencies of the order of 10 GHz that unites this task with a general issue of emergence of slow dynamics from high-energy processes [52]. Another difference is that the spin resonance theory invokes Bloch wave collective excitations propagating over the CSL originated from periodicity of this configuration. However, near the IC-C phase transition the spectrum is undergoing serious changes that are linked to representation of the periodic Lamé potential of the CSL as the sum of Pöschl-Teller potentials localized in space. This necessitates altering the description of spin fluctuations in this regime. More importantly, differential equations of spin dynamics used in the theory of spin resonance [51] describe only linear response of magnetization. To explain the appearance of higher-order harmonics in the magnetic response an another integration scheme of spin dynamics equations should be applied.

In the present study we developed a formalism to describe features of the nonlinear responses revealed in $CrNb_3S_6$ in the vicinity of the IC-C phase transition. We assume that crossover identified experimentally from the weakly nonlinear CSL regime, where the higher-order magnetization harmonics are absent, to the highly nonlinear CSL regime, where they were detected, may be associated with the changing balance between Fourier transforms that make up the static CSL configuration. Another assumption we made is that each of the Pöschl-Teller potentials constituent in the periodic potential of the highly nonlinear CSL covers only a home unit cell of the length L. The problem is then reduced to search of a spectrum of spin fluctuations for the each individual potential and concomitant nonlinear response. A result for the entire system is the sum of these individual contributions.

To implement this approach, we used a Lagrangian description of spin dynamics based on the collective coordinates method, where two dynamical variables are relevant, i.e., one describes a shift in the kink position and the other does a deformation of the kink under such a motion. Interaction between these coordinates and the oscillating magnetic field applied perpendicularly to the chiral axis does determine nonlinear nature of magnetic responses. Employing a

well-developed algorithm for finding periodic solutions of the spin dynamics, we solve the equations of motion in a perturbative manner with respect to the oscillating field. We obtained the higher-order harmonic components of magnetization and concomitant phase shifts originating from higher-order powers of the ac field. The comparison of hierarchy of these contributions with experimental values provides a measure of the kink potential localization L. Thus, we demonstrate that the emergence of higher-order harmonics takes place in a narrow range of steady magnetic fields when there is an optimal distance between the kinks. Moreover, at lower distances, which corresponds to the weakly nonlinear CSL regime, our perturbative scheme is no longer valid. At larger distances (or equivalently, for lower kink density) contributions of the higher-order harmonics become negligible, which confirms restoring of linear response prior to the transition into the ferromagnetic phase [21]. We also mention that at larger distances another type of magnetic interactions (for example, dipole-dipole interaction) may come into play and lower a critical field of the IC-C phase transition. In such a case, metastable kinks may survive in the ferromagnetic phase, nevertheless, the higher-order harmonics will be suppressed in this regime too.

Going back to comparison with the spin resonance measurements, it can be seen that in these experiments the oscillating magnetic field excites standing waves covering the whole system (more exactly, a domain of given chirality). In measurements of nonlinear magnetic responses, according to our theory, such a low-frequency field causes internal deformations of dilute 2π kinks in the highly nonlinear CSL and leads to higher-order harmonics in the magnetic responses.

Some limitations of our analysis should be mentioned. Measurements on thin films of $CrNb_3S_6$ showed that the chiral soliton lattice exhibits magnetic domains extended over 1μm [53]. We ignored this kind of extrinsic domain formation. We also note as well that finite temperature effects on the nonlinear responses and stability of the chiral soliton lattice as a whole [54–56] remain beyond our scope.

ACKNOWLEDGMENTS

The authors would like to express special thanks to Professor Masaki Mito and Professor Hidetoshi Fukuyama for very informative discussions during various stages. The authors also thank Victor Laliena, Javier Campo, and Yusuke Kato for fruitful discussions. This work was supported by JSPS KAKENHI Grant Number 17H02923. A.S.O. acknowledges funding by the Foundation for the Advancement of Theoretical Physics and Mathematics BASIS Grant No. 17-11-107, and by Act 211 Government of the Russian Federation, Contract No. 02.A03.21.0006. A.S.O. thanks also the Ministry of Education and Science of the Russian Federation, Project No. FEUZ-2020-0054.

APPENDIX A: WKB METHOD FOR V_θ

Below, we find the quasistationary levels of a particle in the symmetrical potential shown in Fig. 5 following a general scheme outlined in Ref. [57]. In the region $x < -b$ we have a

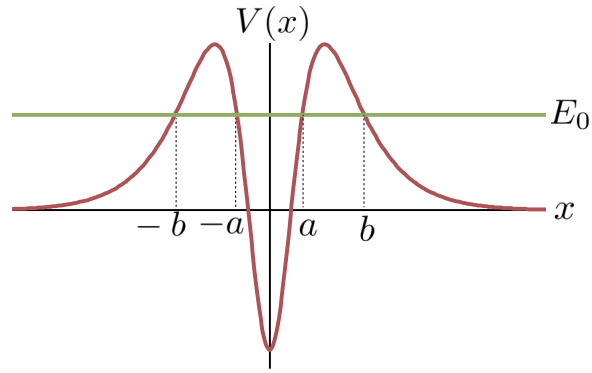

FIG. 5. The inverse double well potential for the WKB analysis.

wave, which goes to $-\infty$,

$$\psi = \frac{c}{\sqrt{p}} \exp\left(\frac{i}{\hbar}\int_x^{-b} p dx\right), \tag{A1}$$

where c is a constant and p is a momentum of the particle. In the region $-b < x < -a$ we obtain

$$\psi = \frac{c}{2\sqrt{|p|}} \exp\left(\frac{i\pi}{4} - \frac{1}{\hbar}\int_{-b}^{-a} |p|dx + \frac{1}{\hbar}\int_x^{-a} |p|dx\right) + \frac{c}{\sqrt{|p|}} \exp\left(-\frac{i\pi}{4} + \frac{1}{\hbar}\int_{-b}^{-a} |p|dx - \frac{1}{\hbar}\int_x^{-a} |p|dx\right). \tag{A2}$$

In the region $-a < x < a$ we get

$$\begin{aligned}\psi = {} & \frac{c}{\sqrt{p}}\left[\frac{1}{4}\exp\left(\frac{i\pi}{2} - \frac{1}{\hbar}\int_{-b}^{-a}|p|dx\right)\right. \\ & \left. + \exp\left(-\frac{i\pi}{2} + \frac{1}{\hbar}\int_{-b}^{-a}|p|dx\right)\right] \\ & \times \exp\left(\frac{i}{\hbar}\int_{-a}^{a} p dx - \frac{i}{\hbar}\int_x^a p dx\right) \\ & \times \frac{c}{\sqrt{p}}\left[\frac{1}{4}\exp\left(-\frac{1}{\hbar}\int_{-b}^{-a}|p|dx\right)\right. \\ & \left. + \exp\left(\frac{1}{\hbar}\int_{-b}^{-a}|p|dx\right)\right] \\ & \times \exp\left(-\frac{i}{\hbar}\int_{-a}^{a} p dx + \frac{i}{\hbar}\int_x^a p dx\right).\end{aligned} \tag{A3}$$

In the region $a < x < b$

$$\begin{aligned}\psi = {} & \frac{c}{\sqrt{|p|}} \exp\left(-\frac{1}{\hbar}\int_a^b |p|dx + \frac{1}{\hbar}\int_x^b |p|dx\right) \\ & \times \left[\sin\left(\frac{1}{\hbar}\int_{-a}^{a} p dx\right)\exp\left(-\frac{i\pi}{4} + \frac{1}{\hbar}\int_{-b}^{-a}|p|dx\right)\right. \\ & \left. + \frac{1}{4}\cos\left(\frac{1}{\hbar}\int_{-a}^{a} p dx\right)\exp\left(\frac{i\pi}{4} - \frac{1}{\hbar}\int_{-b}^{-a}|p|dx\right)\right] \\ & + \frac{c}{\sqrt{|p|}} \exp\left(\frac{1}{\hbar}\int_a^b |p|dx - \frac{1}{\hbar}\int_x^b |p|dx\right)\end{aligned}$$

$$\times\left[-\frac{1}{2}\sin\left(\frac{1}{\hbar}\int_{-a}^{a}pdx\right)\exp\left(\frac{i\pi}{4}-\frac{1}{\hbar}\int_{-b}^{-a}|p|dx\right)\right.$$
$$\left.+\,2\cos\left(\frac{1}{\hbar}\int_{-a}^{a}pdx\right)\exp\left(-\frac{i\pi}{4}+\frac{1}{\hbar}\int_{-b}^{-a}|p|dx\right)\right]. \tag{A4}$$

In the region $x > b$ we find

$$\psi=\frac{c}{\sqrt{p}}\exp\left(\frac{i}{\hbar}\int_{b}^{x}pdx\right)$$
$$\times\left[\frac{1}{8}\exp\left(-\frac{2}{\hbar}\int_{a}^{b}|p|dx+\frac{i\pi}{2}\right)\cos\left(\frac{1}{\hbar}\int_{-a}^{a}pdx\right)\right.$$
$$\left.+2\exp\left(\frac{2}{\hbar}\int_{a}^{b}|p|dx-\frac{i\pi}{2}\right)\cos\left(\frac{1}{\hbar}\int_{-a}^{a}pdx\right)\right]$$
$$+\frac{c}{\sqrt{p}}\exp\left(-\frac{i}{\hbar}\int_{b}^{x}pdx\right)$$
$$\times\left[\frac{1}{8}\exp\left(-\frac{2}{\hbar}\int_{a}^{b}|p|dx\right)\cos\left(\frac{1}{\hbar}\int_{-a}^{a}pdx\right)\right.$$
$$+2\exp\left(\frac{2}{\hbar}\int_{a}^{b}|p|dx\right)\cos\left(\frac{1}{\hbar}\int_{-a}^{a}pdx\right)$$
$$\left.-i\sin\left(\frac{1}{\hbar}\int_{-a}^{a}pdx\right)\right]. \tag{A5}$$

An absence of a wave coming from $+\infty$ yields

$$\cot\left(\frac{1}{\hbar}\int_{-a}^{a}pdx\right)=i\left[\frac{1}{8}\exp\left(-\frac{2}{\hbar}\int_{a}^{b}|p|dx\right)\right.$$
$$\left.+2\exp\left(\frac{2}{\hbar}\int_{a}^{b}|p|dx\right)\right]^{-1}. \tag{A6}$$

Provided $\exp\left(-\frac{2}{\hbar}\int_{a}^{b}|p|dx\right)\ll 1$, we obtain

$$\frac{1}{\hbar}\int_{-a}^{a}pdx=\pi\left(n+\frac{1}{2}\right)-\frac{i}{2}\exp\left(-\frac{2}{\hbar}\int_{a}^{b}|p|dx\right), \tag{A7}$$

where n is a non-negative integer.

The quasistationary levels $E_n^{(0)}$ and their width Γ_n are given by

$$\frac{1}{\hbar}\int_{-a}^{a}\sqrt{2m\left(E_n^{(0)}-V(x)\right)}dx=\pi\left(n+\frac{1}{2}\right), \tag{A8}$$

where $V(x)$ is the potential, m is the mass of the particle, and

$$\Gamma_n=\frac{\hbar\omega}{2\pi}\exp\left(-\frac{2}{\hbar}\int_{a}^{b}|p|dx\right). \tag{A9}$$

Here, ω is the angular frequency of the classical motion in a separate well,

$$\omega=\pi\left(m\int_{-a}^{a}\left\{2m\left[E_n^{(0)}-V(x)\right]\right\}^{-\frac{1}{2}}dx\right)^{-1}.$$

To find $\varepsilon_0^{(\theta)}$ we consider the Schrödinger-like equation

$$\left\{-\frac{1}{2}\frac{d^2}{dz^2}-\frac{3}{\cosh^2 z}+\frac{8}{\pi\cosh z}\right\}u_0(z)=E_0u_0(z) \tag{A10}$$

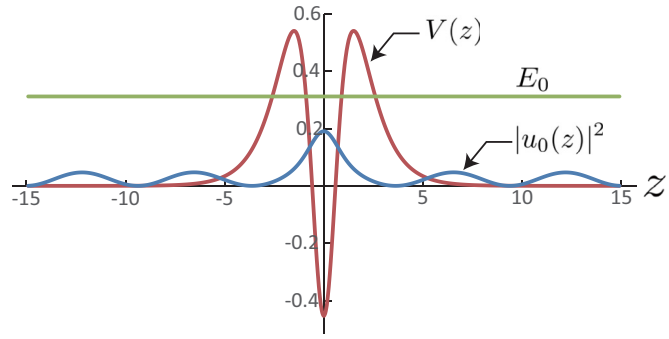

FIG. 6. Spatial profiles of the potential $V(z)$ (red) for the quasilocalized state, the probability density $|u_0(z)|^2$ (blue) and the corresponding energy E_0 (green) obtained by the Numerov's algorithm.

with $E_0=[8\varepsilon_0^{(\theta)}/(\pi q_0 a_0)^2-1/2]$. The energy of the quasilocalized state may be found from (A8) at $n=0$,

$$\int_0^a\sqrt{E_0+\frac{3}{\cosh^2 z}-\frac{8}{\pi\cosh z}}dz=\frac{\pi}{4\sqrt{2}}, \tag{A11}$$

where the upper limit of integration is related with the E_0

$$E_0=-\frac{3}{\cosh^2 a}+\frac{8}{\pi\cosh a}, \tag{A12}$$

which results in $E_0=0.30581$. In Fig. 6 the numerical solution via the Numerov's algorithm is shown [58]. The corresponding E_0 value is 0.31121.

APPENDIX B: ERUGIN'S METHOD

We consider a system of the form

$$\frac{dX}{dt}=X\sum_{k=0}^{\infty}P_k(t)\varepsilon^k, \tag{B1}$$

where $P_k(t)$ are nth-order matrices that are continuous and periodic with period 2π, ε is a small parameter. The integral matrix of Eq. (B1) normalized at the point $t=0$ can be expressed as a series

$$X(t)=\sum_{k=0}^{\infty}X_k(t)\varepsilon^k, \tag{B2}$$

with $X_0(0)=1$, $X_k(0)=0$ at $k\geqslant 1$.

It can be shown (see Ref. [37]) that the integral matrix, giving Floquet solution, can be represented in the form

$$X(t,\varepsilon)=\exp\left[W(\epsilon)t\right]N(t,\varepsilon), \tag{B3}$$

where $W(\epsilon)$ is the real constant matrix and $N(t,\varepsilon)$ is periodic with the period 2π. According to the general theory we have these quantities in the form of the series in powers of ϵ,

$$W(\varepsilon)=\sum_{k=0}^{\infty}W_k\varepsilon^k,\quad N(t,\varepsilon)=\sum_{k=0}^{\infty}N_k(t)\varepsilon^k. \tag{B4}$$

The recipe for finding of the W_k and $N_k(t)$ may be explained as follows. First, we define

$$W_0=\frac{1}{2\pi}\ln[\exp(2\pi P_0)], \tag{B5}$$

and

$$N_0(t) = e^{-W_0 t}\exp(P_0 t). \tag{B6}$$

We can now calculate the periodic matrix $F_k(t)$ with period 2π

$$F_k(t) = \sum_{\nu=1}^{k} N_{k-\nu}(t)P_\nu(t) - \sum_{\nu=1}^{k-1} W_{k-\nu}N_\nu(t). \tag{B7}$$

Then, W_k may be found from

$$\int_0^{2\pi} \exp(P_0 t)F_k N_0^{-1}(t)\exp(-P_0 t)dt = \int_0^{2\pi} \exp(P_0 t)W_k \exp(-P_0 t)dt. \tag{B8}$$

After all, we obtain

$$N_k(t) = \exp(-P_0 t)\left\{\int_0^t \exp(P_0 t')[F_k(t')N_0^{-1}(t') - W_k]\exp(-P_0 t')dt'\right\}\exp(P_0 t)N_0(t). \tag{B9}$$

APPENDIX C: MATRICES W_k AND N_k FOR $k = 2, 3$

Below we result explicitly the matrices W_k and $Z_k(\tau)$, $k = 2, 3$, necessary to build a Floquet solution. By using (B7)–(B9) one may find

$$W_2 = \begin{pmatrix} 0 & \frac{1}{4}\alpha\rho(-6\beta + 5\alpha\rho^2) \\ -\frac{3}{2}\alpha^2\rho & 0 \end{pmatrix}, \quad W_3 = \begin{pmatrix} -\frac{5}{12}(7\alpha^3\rho^3 - 4\alpha^2\beta\rho) & 0 \\ 0 & \frac{5}{12}(7\alpha^3\rho^3 - 4\alpha^2\beta\rho) \end{pmatrix}, \tag{C1}$$

$$N_2(\tau) = \begin{pmatrix} N_{11}^{(2)} & N_{12}^{(2)} \\ N_{21}^{(2)} & N_{22}^{(2)} \end{pmatrix}, \quad N_3(\tau) = \begin{pmatrix} N_{11}^{(3)} & N_{12}^{(3)} \\ N_{21}^{(3)} & N_{22}^{(3)} \end{pmatrix} \tag{C2}$$

with

$$\begin{aligned}
N_{11}^{(2)} &= \tfrac{1}{8}[11\alpha^2\rho^2 - 6\alpha\beta - 16\alpha^2\rho^2\cos\tau + 8\alpha\beta\cos\tau + 5\alpha^2\rho^2\cos 2\tau - 2\alpha\beta\cos 2\tau], \\
N_{12}^{(2)} &= \tfrac{1}{8}[-16\alpha^2\rho^3\sin\tau + 8\alpha\beta\rho\sin\tau + 3\alpha^2\rho^3\sin 2\tau + 2\alpha\beta\rho\sin 2\tau], \\
N_{21}^{(2)} &= \tfrac{1}{4}[4\alpha^2\rho\sin\tau + \alpha^2\rho\sin 2\tau], \\
N_{22}^{(2)} &= \tfrac{1}{8}[17\alpha^2\rho^2 - 6\alpha\beta - 16\alpha^2\rho^2\cos\tau + 8\alpha\beta\cos\tau - \alpha^2\rho^2\cos 2\tau - 2\alpha\beta\cos 2\tau],
\end{aligned}$$

and

$$\begin{aligned}
N_{11}^{(3)} &= \tfrac{1}{72}[153\alpha^3\rho^3\sin\tau + 36\alpha^3\rho^3\sin 2\tau - 5\alpha^3\rho^3\sin 3\tau - 72\alpha^2\beta\rho\sin\tau - 18\alpha^2\beta\rho\sin 2\tau - 4\alpha^2\beta\rho\sin 3\tau], \\
N_{12}^{(3)} &= \tfrac{1}{432}[2284\alpha^3\rho^4 - 1438\alpha^2\beta\rho^2 + 180\alpha\beta^2 - 2187\alpha^3\rho^4\cos\tau - 108\alpha^3\rho^4\cos 2\tau + 11\alpha^3\rho^4\cos 3\tau. \\
&\quad + 1539\alpha^2\beta\rho^2\cos\tau - 162\alpha^2\beta\rho^2\cos 2\tau + 61\alpha^2\beta\rho^2\cos 3\tau - 270\alpha\beta^2\cos\tau + 108\alpha\beta^2\cos 2\tau - 18\alpha\beta^2\cos 3\tau], \\
N_{21}^{(3)} &= \tfrac{1}{48}[98\alpha^3\rho^2 - 20\alpha^2\beta - 129\alpha^3\rho^2\cos\tau + 30\alpha^3\rho^2\cos 2\tau + \alpha^3\rho^2\cos 3\tau + 30\alpha^2\beta\cos\tau - 12\alpha^2\beta\cos 2\tau + 2\alpha^2\beta\cos 3\tau], \\
N_{22}^{(3)} &= \tfrac{1}{144}[-531\alpha^3\rho^3\sin\tau + 54\alpha^3\rho^3\sin 2\tau + \alpha^3\rho^3\sin 3\tau + 144\alpha^2\beta\rho\sin\tau + 36\alpha^2\beta\rho\sin 2\tau + 8\alpha^2\beta\rho\sin 3\tau].
\end{aligned}$$

APPENDIX D: PERIODIC SOLUTIONS

The first pair of the periodic solutions of Eq. (33) has the explicit form

$$\begin{aligned}
\xi_0^{(1)}(\tau) &= 1 + \tfrac{11}{8}\alpha^2\rho^2h_0^2 - \tfrac{3}{4}\alpha\beta h_0^2 + \alpha h_0^2(\beta - 2\alpha\rho^2)\cos\tau + \tfrac{1}{8}\alpha\rho h_0\left(17\alpha^2\rho^2h_0^2 - 8\alpha\beta h_0^2 + 8\right)\sin\tau \\
&\quad + \tfrac{1}{8}\alpha h_0^2(5\alpha\rho^2 - 2\beta)\cos 2\tau + \tfrac{1}{4}\alpha^2\rho h_0^3(2\alpha\rho^2 - \beta)\sin 2\tau - \tfrac{1}{72}\alpha^2\rho h_0^3(5\alpha\rho^2 + 4\beta)\sin 3\tau,
\end{aligned} \tag{D1}$$

$$\begin{aligned}
Z^{(1)}(\tau) &= -\beta h_0 + 2\alpha\rho^2h_0 + \tfrac{5}{12}\alpha\beta^2h_0^3 - \tfrac{719}{216}\alpha^2\beta\rho^2h_0^3 + \tfrac{571}{108}\alpha^3\rho^4h_0^3 \\
&\quad - \tfrac{1}{16}h_0\left(81\alpha^3\rho^4h_0^2 - 57\alpha^2\beta\rho^2h_0^2 + 10\alpha\beta^2h_0^2 + 32\alpha\rho^2 - 16\beta\right)\cos\tau + \alpha\rho h_0^2(\beta - 2\alpha\rho^2)\sin\tau \\
&\quad - \tfrac{1}{8}\alpha h_0^3(2\alpha^2\rho^4 + 3\alpha\beta\rho^2 - 2\beta^2)\cos 2\tau + \tfrac{1}{8}\alpha\rho h_0^2(3\alpha\rho^2 + 2\beta)\sin 2\tau \\
&\quad + \tfrac{1}{432}\alpha h_0^3(11\alpha^2\rho^4 + 61\alpha\beta\rho^2 - 18\beta^2)\cos 3\tau.
\end{aligned} \tag{D2}$$

The second pair may be written as

$$\xi_0^{(2)}(\tau) = \alpha h_0 - \tfrac{5}{12}\alpha^2\beta h_0^3 + \tfrac{49}{24}\alpha^3\rho^2 h_0^3 - \tfrac{1}{16}\alpha h_0\left(43\alpha^2\rho^2 h_0^2 - 10\alpha\beta h_0^2 + 16\right)\cos\tau + \alpha^2\rho h_0^2\sin\tau + \tfrac{1}{8}\alpha^2 h_0^3(5\alpha\rho^2 - 2\beta)\cos 2\tau + \tfrac{1}{4}\alpha^2\rho h_0^2\sin 2\tau + \tfrac{1}{48}\alpha^2 h_0^3(\alpha\rho^2 + 2\beta)\cos 3\tau, \tag{D3}$$

$$Z^{(2)}(\tau) = 1 - \tfrac{3}{4}\alpha\beta h_0^2 + \tfrac{17}{8}\alpha^2\rho^2 h_0^2 + \alpha h_0^2\left(\beta - 2\alpha\rho^2\right)\cos\tau + \left(-\alpha\rho h_0 + \alpha^2\beta\rho h_0^3 - \tfrac{59}{16}\alpha^3\rho^3 h_0^3\right)\sin\tau - \tfrac{1}{8}\alpha h_0^2(\alpha\rho^2 + 2\beta)\cos 2\tau + \tfrac{1}{8}\alpha^2\rho h_0^3(3\alpha\rho^2 + 2\beta)\sin 2\tau + \tfrac{1}{144}\alpha^2\rho h_0^3(\alpha\rho^2 + 8\beta)\sin 3\tau. \tag{D4}$$

The physical solution consistent with the initial condition $\xi_0 = 0, Z = 1$, which means that this is nothing but $\xi_0^{(2)}, Z^{(2)}$.

Bearing in mind that if $X(\tau)$ is the normalized integral matrix at the point $\tau = 0$, i.e., $X(0) = I$, then every other integral matrix $\tilde{X}(\tau)$ can be expressed in the form $\tilde{X}(\tau) = AX(\tau)$, where A is a constant matrix. Therefore, transition to an arbitrary kink position Z_0 is achieved by the matrix $A = \mathrm{diag}\{1, Z_0\}$.

[1] T. Satō and Y. Miyako, J. Phys. Soc. Jpn. **51**, 1394 (1981).
[2] T. Hashimoto, A. Sato, and Y. Fujiwara, J. Phys. Soc. Jpn. **35**, 81 (1973).
[3] L. Rayleigh, Philos. Mag. **23**, 225 (1887).
[4] F. Milstein, J. A. Baldwin, Jr., and M. Rizzuto, J. Appl. Phys. **46**, 4002 (1975).
[5] M. Mito, S. Tominaga, Y. Komorida, H. Deguchi, S. Takagi, Y. Nakao, Y. Kousaka, and J. Akimitsu, J. Phys.: Conf. Ser. **215**, 012182 (2010).
[6] M. Mito, H. Matsui, K. Tsuruta, H. Deguchi, J. Kishine, K. Inoue, Y. Kousaka, S. Yano, Y. Nakao, and J. Akimitsu, J. Phys. Soc. Jpn. **84**, 104707 (2015).
[7] Y. Ishibashi and H. Orihara, Ferroelectrics **156**, 185 (1994).
[8] M. Mito, K. Iriguchi, H. Deguchi, J.-i. Kishine, K. Kikuchi, H. Ohsumi, Y. Yoshida, and K. Inoue, Phys. Rev. B **79**, 012406 (2009).
[9] M. Mito, K. Iriguchi, H. Deguchi, J. Kishine, Y. Yoshida, and K. Inoue, J. Appl. Phys. **111**, 103914 (2012).
[10] M. Suzuki, Prog. Theor. Phys. **58**, 1151 (1977).
[11] Y. Miyako, S. Chikazawa, T. Saito, and Y. G. Yuochunas, J. Phys. Soc. Jpn. **46**, 1951 (1979).
[12] S. Fujiki and S. Katsura, Prog. Theor. Phys. **65**, 1130 (1981).
[13] H. Kawamura, Phys. Rev. Lett. **68**, 3785 (1992).
[14] S. V. Maleyev, Phys. Usp. **45**, 569 (2002).
[15] S. V. Maleyev, Physica B **297**, 67 (2001); **345**, 119 (2004).
[16] H. Kawamura, J. Phys. Soc. Jpn. **79**, 011007 (2010) and references therein.
[17] I. A. Campbell and D. C. M. C. Petit, J. Phys. Soc. Jpn. **79**, 011006 (2010) and references therein.
[18] S. V. Grigoriev, S. V. Maleyev, A. I. Okorokov, Yu. O. Chetverikov, R. Georgii, P. Böni, D. Lamago, H. Eckerlebe, and K. Pranzas, Phys. Rev. B **72**, 134420 (2005).
[19] C. Pappas, E. Lelièvre-Berna, P. Bentley, P. Falus, P. Fouquet, and B. Farago, Phys. Rev. B **83**, 224405 (2011).
[20] K. Tsuruta, M. Mito, H. Deguchi, J. Kishine, Y. Kousaka, J. Akimitsu, and K. Inoue, Phys. Rev. B **93**, 104402 (2016).
[21] E. M. Clements, R. Das, M.-H. Phan, L. Li, V. Keppens, D. Mandrus, M. Osofsky, and H. Srikanth, Phys. Rev. B **97**, 214438 (2018).
[22] N. J. Ghimire, M. A. McGuire, D. S. Parker, B. Sipos, S. Tang, J.-Q. Yan, B. C. Sales, and D. Mandrus, Phys. Rev. B **87**, 104403 (2013).
[23] E. M. Clements, R. Das, L. Li, P. J. Lampen-Kelley, M.-H. Phan, V. Keppens, D. Mandrus, and H. Srikanth, Sci. Rep. **7**, 1 (2017).
[24] Y. Togawa, Y. Kousaka, S. Nishihara, K. Inoue, J. Akimitsu, A. S. Ovchinnikov, and J. Kishine, Phys. Rev. Lett. **111**, 197204 (2013).
[25] V. Laliena, J. Campo, and Y. Kousaka, Phys. Rev. B **94**, 094439 (2016).
[26] V. Laliena, J. Campo, and Y. Kousaka, Phys. Rev. B **95**, 224410 (2017).
[27] P. de Gennes, in *Fluctuations, Instabilities, and Phase Transitions*, edited by T. Riste, NATO ASI Series B Vol. 2 (Plenum, New York, 1975).
[28] Y. A. Izyumov and V. M. Laptev, J. Magn. Magn. Mater. **51**, 381 (1985).
[29] H. Han, L. Zhang, D. Sapkota, N. Hao, L. Ling, H. Du, L. Pi, C. Zhang, D. G. Mandrus, and Y. Zhang, Phys. Rev. B **96**, 094439 (2017).
[30] M. Shinozaki, Y. Masaki, R. Aoki, Y. Togawa, and Y. Kato, Phys. Rev. B **97**, 214413 (2018).
[31] Y. Masaki, arXiv:1912.12677.
[32] J. Rubinstein, J. Math. Phys. **11**, 258 (1970).
[33] B. Sutherland, Phys. Rev. A **8**, 2514 (1973).
[34] J. Kishine and A. S. Ovchinnikov, Solid State Phys. **66**, 1 (2015).
[35] J.-i. Kishine, I. G. Bostrem, A. S. Ovchinnikov, and Vl. E. Sinitsyn, Phys. Rev. B **86**, 214426 (2012).
[36] J.-i. Kishine, I. Proskurin, I. G. Bostrem, A. S. Ovchinnikov, and Vl. E. Sinitsyn, Phys. Rev. B **93**, 054403 (2016).
[37] N. P. Erugin, *Linear Systems of Ordinary Differential Equations with Periodic and Quasi-Periodic Coefficients* (Academic Press, New York, 1966).
[38] Y. Togawa, Y. Kousaka, K. Inoue, and J. Kishine, J. Phys. Soc. Jpn. **85**, 112001 (2016).
[39] T. Moriya and T. Miyadai, J. Phys. Soc. Jpn. **42**, 209 (1982).
[40] T. Miyadai, K. Kikuchi, H. Kondo, S. Sakka, M. Arai, and Y. Ishikawa, J. Phys. Soc. Jpn. **52**, 1394 (1983).
[41] I. E. Dzyaloshinskii, Zh. Eksp. Teor. Fiz. **46**, 1420 (1964) [Sov. Phys. JETP **19**, 960 (1964)]; Zh. Eksp. Teor. Fiz. **47**, 992 (1964) [Sov. Phys. JETP **20**, 665 (1965)].

[42] Y. Togawa, T. Koyama, K. Takayanagi, S. Mori, Y. Kousaka, J. Akimitsu, S. Nishihara, K. Inoue, A. S. Ovchinnikov, and J. Kishine, Phys. Rev. Lett. **108**, 107202 (2012).

[43] Yu. A. Izyumov and V. Laptev, J. Exp. Theor. Phys. **58**, 1267 (1983).

[44] We note that in the weakly nonlinear regime $\varphi_0(z) \approx \pi + q_0 z + \frac{\kappa^2}{4} \sin(q_0 z)$, whereas in the highly nonlinear regime, when κ goes to 1, it becomes incorrect and higher-order harmonics associated with C_n ($n \neq \pm 1$) come into play, wherein the zero-order component, or C_0, dominates.

[45] J. Müller, A. Rosch, and M. Garst, New J. Phys. **18**, 065006 (2016).

[46] J.-i. Kishine and A. S. Ovchinnikov, Phys. Rev. B **81**, 134405 (2010).

[47] W. Döring, Z. Naturforschung **3a**, 373 (1948).

[48] The damping effect may be incorporated into the formalism by defining the new variables $\tilde{\xi}_0 = \xi_0 + \frac{\gamma \hbar S \mathcal{M}}{K_1 a_0} Z$ and $\tilde{Z} = Z - \frac{\gamma \hbar S \mathcal{M}}{K_1 a_0} \xi_0$, and keeping terms of equations of motion linear in either γ or h_0.

[49] F. J. T. Goncalves, T. Sogo, Y. Shimamoto, Y. Kousaka, J. Akimitsu, S. Nishihara, K. Inoue, D. Yoshizawa, M. Hagiwara, M. Mito, R. L. Stamps, I. G. Bostrem, V. E. Sinitsyn, A. S. Ovchinnikov, J. Kishine, and Y. Togawa, Phys. Rev. B **95**, 104415 (2017).

[50] F. J. T. Goncalves, T. Sogo, Y. Shimamoto, I. Proskurin, Vl. E. Sinitsyn, Y. Kousaka, I. G. Bostrem, J. Kishine, A. S. Ovchinnikov, and Y. Togawa, Phys. Rev. B **98**, 144407 (2018).

[51] J. Kishine, Vl. E. Sinitsyn, I. G. Bostrem, I. Proskurin, F. J. T. Gonsalves, Y. Togawa, and A. S. Ovchinnikov, Phys. Rev. B **100**, 024411 (2019).

[52] H. Fukuyama, J. Kishine, and M. Ogata, J. Phys. Soc. Jpn. **86**, 123706 (2017).

[53] Y. Togawa, T. Koyama, Y. Nishimori, Y. Matsumoto, S. McVitie, D. McGrouther, R. L. Stamps, Y. Kousaka, J. Akimitsu, S. Nishihara, K. Inoue, I. G. Bostrem, Vl. E. Sinitsyn, A. S. Ovchinnikov, and J. Kishine, Phys. Rev. B **92**, 220412(R) (2015).

[54] J. A. Krumhansl and J. R. Schrieffer, Phys. Rev. B **11**, 3535 (1975).

[55] N. Gupta and B. Sutherland, Phys. Rev. A **14**, 1790 (1976).

[56] M. Shinozaki1, S. Hoshino, Y. Masaki, J. Kishine, and Y. Kato, J. Phys. Soc. Jpn. **85**, 074710 (2016).

[57] D. ter Haar, *Selected Problems in Quantum Mechanics* (Infosearch Limited, London, 1964).

[58] R. H. Landau, M. J. Páez, and C. C. Bordeianu, *A Survey of Computational Physics* (Princeton University Press, Princeton, 2008).